A Journal of the Gesellschaft Deutscher Chemiker

Angewandte International Edition

GDCh

Chemie

www.angewandte.org

Accepted Article

Title: Highly Selective Electrochemical Reduction of CO2 to Alcohols on FeP Nanoarray

Authors: Xuping Sun

This manuscript has been accepted after peer review and appears as an Accepted Article online prior to editing, proofing, and formal publication of the final Version of Record (VoR). This work is currently citable by using the Digital Object Identifier (DOI) given below. The VoR will be published online in Early View as soon as possible and may be different to this Accepted Article as a result of editing. Readers should obtain the VoR from the journal website shown below when it is published to ensure accuracy of information. The authors are responsible for the content of this Accepted Article.

To be cited as: *Angew. Chem. Int. Ed.* 10.1002/anie.201912836
Angew. Chem. 10.1002/ange.201912836

Link to VoR: http://dx.doi.org/10.1002/anie.201912836
http://dx.doi.org/10.1002/ange.201912836

WILEY-VCH

10.1002/anie.201912836

WILEY-VCH

Highly Selective Electrochemical Reduction of CO_2 to Alcohols on FeP Nanoarray

Lei Ji,[†a,b] Lei Li,[†c] Xuqiang Ji,[†a] Ya Zhang,[a,b] Shiyong Mou,[a] Tongwei Wu,[a] Qian Liu,[a] Baihai Li,[c] Xiaojuan Zhu,[a,d] Yonglan Luo,[d] Xifeng Shi,[e] Abdullah M. Asiri,[f] and Xuping Sun*[a]

Abstract: Electrochemical reduction of CO_2 into various chemicals and fuels provides an attractive pathway for environmental and energy sustainability. In this communication, we report on our recent experimental finding that FeP nanoarray on Ti mesh (FeP NA/TM) acts as an efficient 3D catalyst electrode for the CO_2 reduction reaction to convert CO_2 to alcohols with high selectivity. In 0.5 M $KHCO_3$, such FeP NA/TM is capable of achieving a high Faradaic efficiency (FE_{CH3OH}) up to 80.2%, with a total $FE_{CH3OH+C2H5OH}$ of 94.3% at −0.20 V vs. reversible hydrogen electrode. Density functional theory calculations reveal that the FeP(211) surface significantly promotes the adsorption and reduction of CO_2 toward CH_3OH due to the synergistic effect of two adjacent Fe atoms and the potential-determining step is the hydrogenation process of *CO.

The massive comsuption of fossil fuels has led to an escalation in atmospheric CO_2 concentrations and such CO_2 emissions trap solar energy within the Earth's atmosphere, which are responsible for global climate change.[1,2] To struggle against the greenhouse effect, research efforts have been extensively made to develop technologies for capturing CO_2 and sequestering or utilizing it. Several routes have been explored to transform CO_2 into other carbon compounds so far, including chemical reforming,[3–5] photochemical,[6–9] biological,[10–12] and electrochemical[13–17] methods. Among them, electrocatalytic reduction has emerged as an attractive way to resolve environmental and energy issues.[18–21] For most electrocatalysts, however, the inertness of CO_2 molecules and complex multi-electron transfer steps involved in CO_2 reduction reaction (CO_2RR) result in large thermodynamic barriers, slow kinetics and low Faraday efficiency (FE) and selectivity toward specific products. In this regard, it is needed to develop highly selective and efficient electrocatalysts for CO_2RR.

Fe is the cheapest and one of the most abundant of all transition metals[22] and thus may hold great promise as a low-cost catalyst material for large-scale uses. Iron macrocyclic complexes represent one of the most extensively researched categories of molecular catalysts for selective CO_2 reduction to CO.[23] Because of the synthetic issues of such complexes, it is challenging to effectively immobilize them onto electrodes for practical application, which can be avoided by heterogeneous alternatives.[24–27] Porous Fe_3N single crystal was reported to yield CO with a selectivity of 90%.[24] Tour and co-workers developed atomic iron dispersed on nitrogen-doped graphene for CO_2RR with a FE for CO of 80%.[25] Singly-dispersed FeN_5 active sites supported on N-doped graphene enables CO_2-to-CO conversion with a FE of ~97.0%.[26] Recent study suggests that discrete Fe^{3+} ions coordinated to pyrrolic nitrogen atoms of the N-doped carbon support have ultrahigh activity for CO_2 electroreduction to CO.[27] Compared with CO, alcohols possesse advantages of higher energy density and easier storage at atmospheric pressure, and they are also widely used to feed the direct alcohols fuel cells.[28–30] Therefore, it is highly attractive but still remains a big challenge to achieve efficient electrocatalytic CO_2 reduction to alcohols with high selectivity.

In this communication, we report the direct utilization of FeP nanoarray on Ti mesh (FeP NA/TM) as an efficient 3D catalyst electrode to electrochemically convert CO_2 to alcohols. In 0.5 M $KHCO_3$, the FeP NA/TM offers a high FE_{CH3OH} up to 80.2%, with a total $FE_{CH3OH+C2H5OH}$ of 94.3% at −0.20 V vs. reversible hydrogen electrode (RHE). It also shows a remarkably high stability during 36 h continuous electrocatalysis. Density functional theory (DFT) calculations reveal that the FeP(211) surface significantly promotes the adsorption and reduction of CO_2 toward CH_3OH due to the synergistic effect of two adjacent Fe atoms and the hydrogenation process of *CO is the potential-determining step (PDS) with a free energy of 0.76 eV.

FeP NA/TM was derived from Fe_2O_3 NA/TM via our well-established topotactic conversion process.[31] The X-ray diffraction (XRD) pattern (Figure S1) for the precursor scratched from TM shows characteristic peaks of Fe_2O_3 (JCPDS No. 84-0306). The scanning electron microscopy (SEM) image indicates that the surface of TM is coated with Fe_2O_3 nanorod array (Figure S2). Following phosphidation, the product presents characteristic diffraction peaks indexed to the (011), (111), (202), (211), (103), (212), (020), and (114) planes of FeP phase (JCPDS No. 78-1443), as shown in Figure 1a. Note that the FeP product well maintains the nanoarray feature (Figure 1b). As shown in Figure 1c, the transmission electron microscopy (TEM) image further indicates the nanorod nature of FeP. The high-resolution TEM (HRTEM) image (Figure 1d) taken from one single FeP nanorod reveals clear lattice fringes with an interplanar distance of 0.18 nm corresponding to the (211) plane of FeP. The energy dispersive X-ray (EDX) spectrum shows the presence of Fe and P elements with the atomic ratio of nearly 1:1, as shown in Figure S3. The scanning TEM (STEM) and corresponding EDX elemental mapping images (Figure 1e)

[a] L. Ji, Dr. X. Ji, Y. Zhang, S. Mou, T. Wu, Dr. Q. Liu, X. Zhu, Prof. X. Sun Institute of Fundamental and Frontier Sciences, University of Electronic Science and Technology of China, Chengdu 610054, Sichuan (China)
E-mail: xpsun@uestc.edu.cn
[b] L. Ji, Y. Zhang
College of Chemistry, Sichuan University, Chengdu 610064, Sichuan (China)
[c] L. Li, Prof. B. Li
School of Materials and Energy, University of Electronic Science and Technology of China, Chengdu 611731, Sichuan (China)
[d] X. Zhu, Y. Luo
Chemical Synthesis and Pollution Control Key Laboratory of Sichuan Province, College of Chemistry and Chemical Engineering, China West Normal University, Nanchong 637002, Sichuan (China)
[e] Dr. X. Shi
College of Chemistry, Chemical Engineering and Materials Science, Shandong Normal University, Jinan 250014, Shandong (China)
[f] Prof. A. M. Asiri
Chemistry Department, Faculty of Science & Center of Excellence for Advanced Materials Research, King Abdulaziz University, P.O. Box 80203, Jeddah 21589 (Saudi Arabia)

[†]These authors contributed equally to this work.
Supporting information for this article is given via a link at the end of the document.

Accepted Manuscript

This article is protected by copyright. All rights reserved.

further confirm the uniform distribution of Fe and P elements. All above results strongly support the successful preparation of FeP NA/TM.

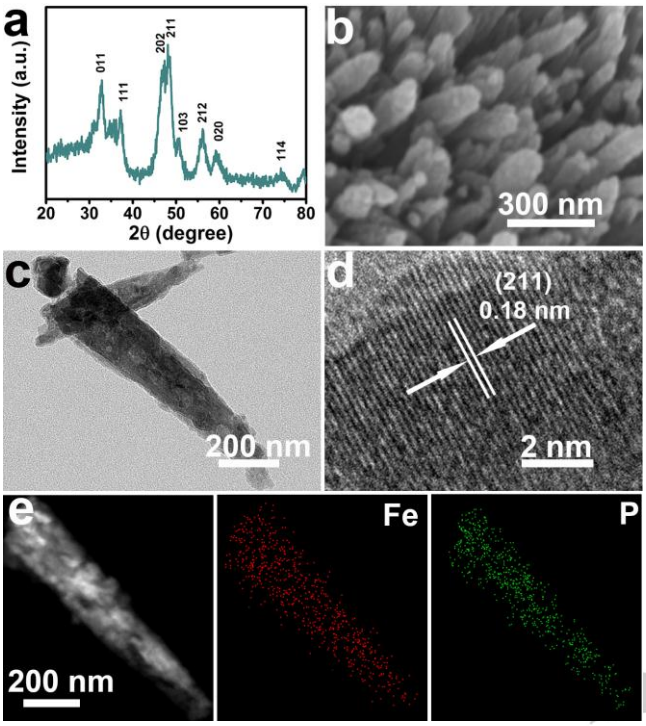

Figure 1. (a) XRD pattern for FeP scratched from TM. (b) SEM image for FeP NA/TM. (c) TEM and (d) HRTEM images taken from FeP nanorod. (e) STEM image of FeP nanorod and EDX elemental mapping of Fe and P.

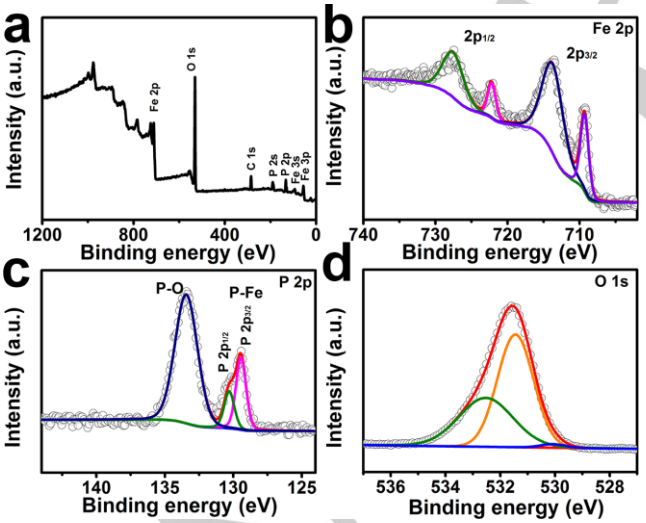

Figure 2. (a) XPS survey spectrum of FeP. XPS spectra in the (b) Fe 3d, (c) P 2p, and (d) O 1s regions for FeP.

The X-ray photoelectron spectroscopy (XPS) survey spectrum for FeP (Figure 2a) shows the peaks of Fe and P with signals of C and O elements due to contamination/surface oxidation of the product.[32] In the Fe 2p spectra (Figure 2b), two binding energies at 706.5 and 719.3 eV correspond to $2p_{3/2}$ and $2p_{1/2}$ in FeP, respectively, and the two peaks at 710.6 and 724.1 eV are ascribed to Fe-O.[33] The peaks at 713.9 and 727.8 eV are well fitted with two shakeup satellites.[33] The P 2p region (Figure 2c) shows two peaks at 128.9 and 129.7 eV assigned to P $2p_{3/2}$ and $2p_{1/2}$ in FeP and the P-O species stem from surface oxidation of P in FeP after exposure to air.[32,33] In the O 1s region (Figure 2d), the fitted peaks at 530.1, 531.4, and 532.6 eV are ascribed to lattice O, adsorbed O from surface hydroxy and/or adsorbed oxygen species, and O from the surface of absorbed H_2O, respectively.[34]

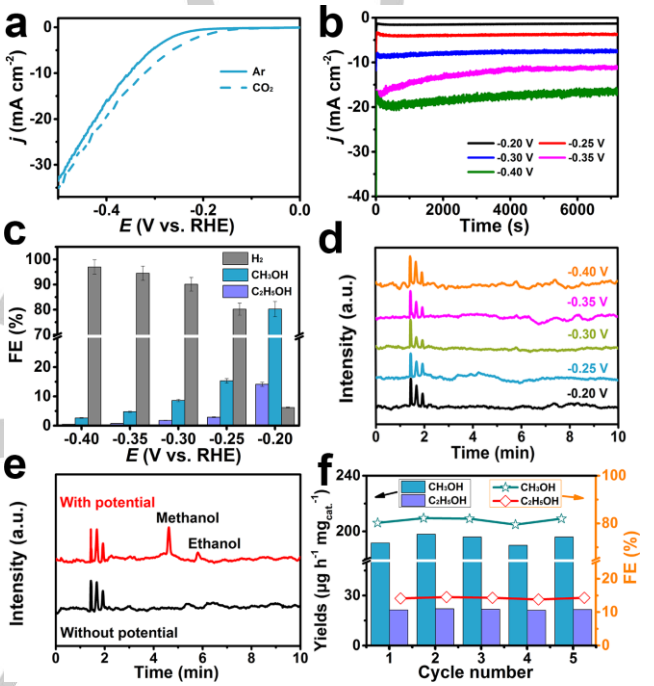

Figure 3. (a) LSV curves of FeP NA/TM in Ar- or CO_2-saturated 0.5 M $KHCO_3$ solution. (b) Chronoamperometry curves of CO_2RR over FeP NA/TM in 0.5 M $KHCO_3$ solution at different potentials (error bars represent the standard deviation of five measurements). (c) FEs of CO_2RR products on FeP NA/TM at different potentials. (d) Chromatograms for Ar-saturated 0.5 M $KHCO_3$ at different potentials using HS-GC. (e) Chromatograms for CO_2-saturated 0.5 M $KHCO_3$ with and without potential applied to the electrochemical cell. (f) Alcohols yields and FEs on FeP NA/TM at applied potential –0.20 V for 5 times cycle measurements.

We evaluated the catalytic CO_2RR performance of the FeP NA/TM using a three-electrode system. The potentials for CO_2RR are all reported on a RHE scale. Figure 3a presents the linear sweep voltammetry (LSV) curves for FeP NA/TM in Ar- and CO_2-saturated 0.5 M $KHCO_3$. Obviously, a higher cathodic current density can be clearly seen in CO_2-saturated electrolyte on FeP NA/TM, indicating the occurrence of CO_2RR. According to the polarization curves, the appropriate potential window for electrocatalytic CO_2RR ranges from −0.20 to −0.40 V. Figure 3b shows the chronoamperometry curves at different applied potentials, in which the steady current densities suggest good electrochemical stability of FeP NA/TM during CO_2RR tests. To identify the CO_2 reduction products, on-line gas chromatography

Accepted Manuscript

This article is protected by copyright. All rights reserved.

(GC) and headspace GC (HS-GC) analyses were performed to quantify the gaseous and liquid products (Figure S4 and S5). The FEs at various potentials is calculated and shown in Figure 3c, respectively. As observed, the FE of alcohols achieves the maximum value of 94.3% (FE_{CH3OH}: 80.2%; FE_{C2H5OH}: 14.1%) at –0.20 V. Here, note that the value of CH_3OH is higher than those for $Fe_2P_2S_6$ nanosheet (65.2%)[35] and other electrocatalysts (see Table S1). It is worth while mentioning that no CO_2RR products were detected on Fe_2O_3 NA/TM within the investigated potential window (Table S2).

Control experiments were performed to further confirm that CH_3OH and C_2H_5OH were indeed generated by electrochemical reduction of CO_2 over FeP NA/TM. In Ar-saturated 0.5 M $KHCO_3$, there is no CH_3OH and C_2H_5OH at different potentials (Figure 3d). CH_3OH and C_2H_5OH were not detected when no potential was applied to CO_2-saturated electrolyte (Figure 3e). ^1H nuclear magnetic resonance (NMR) data (Figure S6) prove the formation of CH_3OH and C_2H_5OH during CO_2RR process. Isotope labeled $^{13}CO_2$ was also used as feeding gas to trace the origin of carbon source. As we can see in Figure S7, the incorporation of the ^{13}C label into CH_3OH was proved by the peak splitting shown in ^1H NMR,[36] which provides direct evidence to show that CH_3OH in the system only originate from electrochemical CO_2RR over the FeP NA/TM. All results provide clear evidence to support that alcohols product in the system only stem from electrochemical CO_2RR over FeP NA/TM. Ion chromatography (IC) analysis (Figure S8) also indicates that no $HCOO^-$ products formed over FeP NA/TM at all potentials. Meanwhile it is safely to conclude that electrocatalytic CO_2RR over FeP NA/TM only produces CH_3OH, C_2H_5OH, and H_2 without the formation of $HCOO^-$, CH_4, and CO.

Stability is also a critical parameter of CO_2RR performance for practical applications. FeP NA/TM shows no obvious attenuation in yield and FE during consecutive recycling tests at −0.20 V for 5 times (Figure 3f). Furthermore, under sustained CO_2 gas flow in cathode, 36-h electrolysis at a potential of −0.20 V only leads to a slight decrease in current density (Figure S9). Compared with the initial one, the yields of CH_3OH and C_2H_5OH for FeP NA/TM exhibits only 7% decrease (Figure S10) after long-term electrolysis, indicating that high electrocatalytic activity for CO_2RR is maintained.

DFT calculations were performed to gain further insight into the catalytic mechanism. Based on the XRD and HRTEM data, FeP(211) surface is considered. Firstly, CO_2 molecule is adsorbed on the two adjacent surface Fe atoms by side-on coordination with a free energy change (ΔG) of −0.40 eV, and it can be seen that carbon atom and one of oxygen atom in CO_2 molecule interact with Fe atoms respectively, as shown in Figure 4. Bader charge analysis shows that CO_2 molecule is transferred into 0.69 e^- from FeP(211) surface, implying that it is effectively activated. Subsequently, the hydrogenation process of CO_2 is proceeded. The first hydrogenation of $*CO_2$ prefers to take place on the tilted oxygen atom (*COOH) with ΔG = −0.31 eV. Then, the hydrogenation of *COOH should occur at the same oxygen atom to form H_2O molecule and *CO with ΔG = −0.31 eV, as shown in Figure 4. Next, hydrogenation processes of *CO to *COH and *COH to *CHOH are uphill pathway with ΔG = 0.76 and 0.70 eV respectively, and then *CHOH is hydrogenated to $*CH_2OH$ with a downhill pathway of ΔG = −0.12 eV. The hydrogenation process of $*CH_2OH$ to $*CH_3OH$ is an uphill pathway with ΔG = 0.28 eV, and surprisingly the $*CH_3OH$ desorption is exothermic process with ΔG = −0.26 eV. For this case, it suggests that the hydrogenation of *CO to *COH is the PDS with ΔG = 0.76 eV while the *COH desorption is difficult because C atom in *COH is fixed by two adjacent Fe atoms. On the other pathway, double *CO adsorption is considered and results show that it is a downhill pathway, which is advantage to form C_2H_5OH. However, the hydrogenation is difficult with ΔG = 1.33 eV, implying that the formation of double carbon (C_2) intermediate (*CO-*COH) is not preferable. Moreover, the next hydrogenation is also difficult with ΔG = 1.20 eV. Then, the rest hydrogenation steps are facile due to exothermic process or endothermic process consuming a small energy, while the entire reaction processes were presented in Figure S11. The PDS for C_2H_5OH pathway is much higher than that of the CH_3OH pathway, suggesting that Fe(211) surface more prefers to produce CH_3OH, which is consistent with experiment results. Overall, the PDS for CH_3OH production is *CO to *COH process with ΔG = 0.76 eV, which is comparable with that on the well-established Cu(211) with ΔG = 0.74 eV.[37]

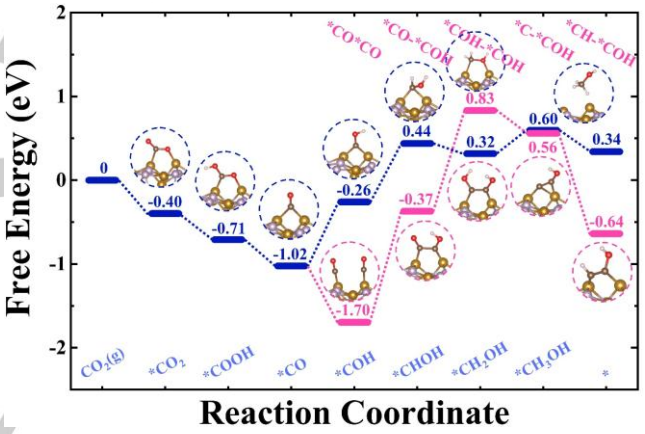

Figure 4. Free energy diagram for CO_2RR process occurring on FeP(211). Asterisk (*) denotes the adsorbed intermediate. The CH_3OH and C_2H_5OH synthesis reaction processes are drawn in blue and pink, respectively, with the intermediated configurations.

To get a deep insight of the significant HER suppression on the FeP(211) surface, ΔG_{*H} on different reaction sites have been calculated. As shown in Figure S12, four possible sites including Fe-1, Fe-2, P-1 and P-2 were taken into consideration. The calculated ΔG_{*H} are 0.08, 0.16, 0.39 and 0.50 eV for Fe-1, Fe-2, P-1 and P-2, respectively, as presented in Figure S13. Obviously, the Fe sites are the most ideal active sites for HER due to these values of ΔG_{*H} are most close to zero. However, the Fe sites might be occupied by CO_2 molecule because of the much stronger binding interactions with the ΔG_{*CO2} of −0.40 eV. In addition, the rate for *CO formation reaches its maximum at the onset potential for HER.[38] When the potential is below −0.20 V, the decrease of *CO formation when the occurrence of HER is attributed to the limited available sites, which further affects the hydrogenation of CO_2. In addition, the potential has little effect on the chemical adsorption of CO, whereas the electrochemical adsorption of H^+ is determined by the potential

Accepted Manuscript

This article is protected by copyright. All rights reserved.

value.[39] Therefore, when the potential is below –0.20 V, FEs of CO_2RR decrease and HER increase obviously.

In summary, FeP nanoarray is verified experimentally as a superb electrocatalyst for CO_2RR toward alcohols production with high stability, capable of attaining a FE_{CH3OH} up to 80.2% with a total $FE_{CH3OH+C2H5OH}$ of 94.3% at −0.20 V vs. RHE. Theoretical studies further suggest that the synergistic effect of two adjacent Fe atoms on FeP(211) surface favors the adsorption and reduction of CO_2 to CH_3OH and the potential-determining step is the hydrogenation process of *CO with a free energy of 0.76 eV. The whole fabrication process is cost-effective and easy to scale-up. This feature, together with its remarkable catalytic performances, promises its use as an attractive earth-abundant catalyst material for CO_2RR toward alcohol electrosynthesis.

Acknowledgement

This work was supported by the National Natural Science Foundation of China (No. 21575137). We also appreciate Hui Wang from the Analytical & Testing Center of Sichuan University for her help with SEM characterization.

Keywords: FeP • CO_2 reduction reaction • electrocatalysts • alcohols • density functional theory

[1] S. S. Myers, K. R. Wessells, I. Kloog, A. Zanobetti, J. Schwartz, *Lancet Glob. Health* **2015**, *3*, e639–e645.
[2] D. R. Feldman, W. D. Collins, P. J. Gero, M. S. Torn, E. J. Mlawer, T. R. Shippert, *Nature* **2015**, *519*, 339–343.
[3] J. Graciani, K. Mudiyanselage, F. Xu, A. E. Baber, J. Evans, S. D. Senanayake, D. J. Stacchiola, P. Liu, J. Hrbek, J. F. Sanz, J. A. Rodriguez, *Science* **2014**, *345*, 546.
[4] J. Ma, N. Sun, X. Zhang, N. Zhao, F. Xiao, W. Wei, Y. Sun, *Catal. Today* **2009**, *148*, 221–231.
[5] X. Pan, Z. Fan, W. Chen, Y. Ding, H. Luo, X. Bao, *Nat. Mater.* **2007**, *6*, 507.
[6] T. Ouyang, H.-H. Huang, J.-W. Wang, D.-C. Zhong, T.-B. Lu, *Angew. Chem. Int. Ed.* **2017**, *56*, 738–743.
[7] X. Chang, T. Wang, P. Zhang, Y. Wei, J. Zhao, J. Gong, *Angew. Chem. Int. Ed.* **2016**, *55*, 8840–8845.
[8] S. Sato, T. Morikawa, T. Kajino, O. Ishitani, *Angew. Chem. Int. Ed.* **2013***, 52,* 988–992.
[9] S. Sato, T. Morikawa, S. Saeki, T. Kajino, T. Motohiro, *Angew. Chem. Int. Ed.* **2010***, 49,* 5101–5105.
[10] K. Schuchmann, V. Müller, *Science* **2013**, *342*, 1382–1385.
[11] M. Mondal, S. Khanra, O. N. Tiwari, K. Gayen, G. N. Halder, *Environ. Prog. Sustainable Energy* **2016**, *35*, 1605–1615.
[12] A. M. Appel, J. E. Bercaw, A. B. Bocarsly, H. Dobbek, D. L. DuBois, M. Dupuis, J. G. Ferry, E. Fujita, R. Hille, P. J. A. Kenis, C. A. Kerfeld, R. H. Morris, C. H. F. Peden, A. R. Portis, S. W. Ragsdale, T. B. Rauchfuss, J. N. H. Reek, L. C. Seefeldt, R. K. Thauer, G. L. Waldrop, *Chem. Rev.* **2013**, *113*, 6621–6658.
[13] A. Vasileff, C. Xu, Y. Jiao, Y. Zheng, S.-Z. Qiao, *Chem* **2018**, *4*, 1809–1831.
[14] L. Zhang, Z.-J. Zhao, J. Gong, *Angew. Chem. Int. Ed.* **2017**, *56*, 11326–11353.
[15] W. Zhang, Q. Qin, L. Dai, R. Qin, X. Zhao, X. Chen, D. Ou, J. Chen, T. Chuong, B. Wu, N. Zheng, *Angew. Chem. Int. Ed.* **2018**, *57*, 9475–9479.
[16] C. Chen, J. F. K. Kotyk, S. W. Sheehan, *Chem* **2018**, *4*, 2571–2586.
[17] J. Qiao, Y. Liu, F. Hong, J. Zhang, *Chem. Soc. Rev.* **2014**, *43*, 631–675.
[18] E. V. Kondratenko, G. Mul, J. Baltrusaitis, G. O. Larrazábal, J. Pérez-Ramírez, *Energy Environ. Sci.* **2013**, *6*, 3112–3135.
[19] D. Zhu, J. Liu, S. Qiao, *Adv. Mater.* **2016**, *28*, 3423–3452.
[20] X. Duan, J. Xu, Z. Wei, J. Ma, S. Guo, S. Wang, H. Liu, S. Dou, *Adv. Mater.* **2017**, *29*, 1701784.
[21] H. Xie, T. Wang, J. Liang, Q. Li, S. Sun, *Nano Today* **2018**, *21*, 41–54.
[22] P. Jiang, Q. Liu, Y. Liang, J. Tian, A. M. Asiri, X. Sun, *Angew. Chem. Int. Ed.* **2014***, 53,* 12855–12859.
[23] K. Elouarzaki, V. Kannan, V. Jose, H. S. Sabharwal, J.-M. Lee, *Adv. Energy Mater.* **2019**, *9*, 1900090.
[24] F. Zhang, S. Xi, G. Lin, X. Hu, X. W. Lou, K. Xi, *Adv. Mater.* **2019**, *31*, 1806552.
[25] C. Zhang, S. Yang, J. Wu, M. Liu, S. Yazdi, M. Ren, J. Sha, J. Zhong, K. Nie, A. S. Jalilov, Z. Li, H. Li, B. I. Yakobson, Q. Wu, E. Ringe, H. Xu, P. M. Ajayan, J. M. Tour, *Adv. Energy Mater*. **2018**, *8*, 1703487.
[26] H. Zhang, J. Li, S. Xi, Y. Du, X. Hai, J. Wang, H. Xu, G. Wu, J. Zhang, J. Lu, J. Wang, *Angew. Chem. Int. Ed.* **2019**, DOI: 10.1002/ange.201906079.
[27] J. Gu, C.-S. Hsu, L. Bai, H. M. Chen, X. Hu, *Science* **2019**, *364*, 1091–1094.
[28] N. Kakati, J. Maiti, S. H. Lee, S. H. Jee, B. Viswanathan, Y. S. Yoon, *Chem. Rev.* **2014**, *114*, 12397–12429.
[29] M. A. Z. G. Sial, M. A. U. Dina, X. Wang, *Chem. Soc. Rev.* **2018***, 47*, 6175–6200.
[30] F. Jia, X. Yu, L. Zhang, *J. Power Sources* **2014**, *252*, 85–89.
[31] J. Tian, Q. Liu, A. M. Asiri, X. Sun, *J. Am. Chem. Soc.* **2014**, *136*, 7587–7590.
[32] T. Liu, D. Liu, F. Qu, D. Wang, L. Zhang, R. Ge, S. Hao, Y. Ma, G. Du, A. M. Asiri, L. Chen, X. Sun, *Adv. Energy Mater*. **2017**, *7*, 1700020.
[33] X. Peng, A. M. Qasim, W. Jin, L. Wang, L. Hu, Y. Miao, W. Li, Y. Li, Z. Liu, K. Huo, K. Wong, P. K. Chu, *Nano Energy* **2018**, *53*, 66–73.
[34] Z. Wang, H. Liu, R. Ge, X. Ren, J. Ren, D. Yang, L. Zhang, X. Sun, *ACS Catal.* **2018**, *8*, 2236–2241.
[35] L. Ji, L. Chang, Y. Zhang, S. Mou, T. Wang, Y. Luo, Z. Wang, X. Sun, *ACS Catal.* **2019**, *9*, 9721–9725.
[36] K. P. Kuhl, T. Hatsukade, E. R. Cave, D. N. Abram, J. Kibsgaard, T. F. Jaramillo, *J. Am. Chem. Soc.* **2014**, *136*, 14107–14113.
[37] A. A. Peterson, F. Abild-Pedersen, F. Studt, J. Rossmeisl, J. K. Nørskov, *Energy Environ. Sci.* **2010**, *3*, 1311–1315.
[38] J. Yang, J. Wei, W. Chen, Y. Chen, *Chin. J. Chem. Phys.* **2018**, *31*, 626−634.
[39] Z. Chen, W. Gao, W. Zheng, Q. Jiang, *ChemSusChem* **2018**, *11*, 1455–1459.

Accepted Manuscript

This article is protected by copyright. All rights reserved.

10.1002/anie.201912836

COMMUNICATION

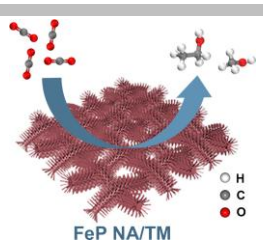

FeP nanoarray on Ti mesh (FeP NA/TM) performs efficiently to electrocatalyze CO_2 reduction to alcohols with a high Faradaic efficiency (FE_{CH3OH}) up to 80.2% and a total $FE_{CH3OH+C2H5OH}$ of 94.3% at −0.20 V vs. reversible hydrogen electrode. Density functional theory calculations reveal that the FeP(211) surface significantly promotes the adsorption and reduction of CO_2 toward CH_3OH due to the synergistic effect of two adjacent Fe atoms and the potential-determining step is the hydrogenation process of *CO.

Lei Ji,[†[a,b]] Lei Li,[†[c]] Xuqiang Ji,[†[a]] Ya Zhang,[[a,b]] Shiyong Mou,[[a]] Tongwei Wu,[[a]] Qian Liu,[[a]] Baihai Li,[[c]] Xiaojuan Zhu,[[a,d]] Yonglan Luo,[[d]] Xifeng Shi,[[e]] Abdullah M. Asiri,[[f]] and Xuping Sun[[a]]*

Page No. – Page No.

Highly Selective Electrochemical Reduction of CO_2 to Alcohols on FeP Nanoarray

WILEY-VCH

Accepted Manuscript

This article is protected by copyright. All rights reserved.